Enhancing Stability and Efficiency of Perovskite Solar Cells Using Graphene-Based Metamaterials

Zhicheng Zheng *

College of Physics & Technology, HeBei University, BaoDing, China, 071002

* Corresponding Author Email: zzc1963517795@163.com

Abstract. Against the backdrop of energy shortages, perovskite solar cells have developed rapidly, with their photoelectric conversion efficiency increasing from an initial 3.8% to 26.4%. However, the issue of device stability severely limits their practical applications. Graphene, with its excellent optoelectronic properties, The carbon-based perovskite solar cells based on Ti_1–rGO have achieved a photovoltaic conversion efficiency of up to 20.6% under steady-state conditions, indicating that graphene contributes to enhancing the stability of the cells. However, the issue of hysteresis still persists. To address this problem, this paper designs a highly efficient and stable perovskite solar cell based on graphene metamaterials. By suppressing ion migration probability, the stability of the device is remarkably promoted, and the photoelectric conversion efficiency is stabilized at 19.7%-25.9% (310 K-100 K).

Keywords: Perovskite solar cells, graphene-based metamaterials, ion migration.

1. Introduction

With the quick development of heavy industry, energy issues have become increasingly severe, drawing growing attention to renewable energy sources such as solar energy. The photoelectric conversion efficiency of traditional amorphous silicon solar cells has shown slow improvement. In contrast, perovskite solar cells have advanced quickly, with their conversion efficiency rising from an initial 3.8%to 26.4% [1-8].

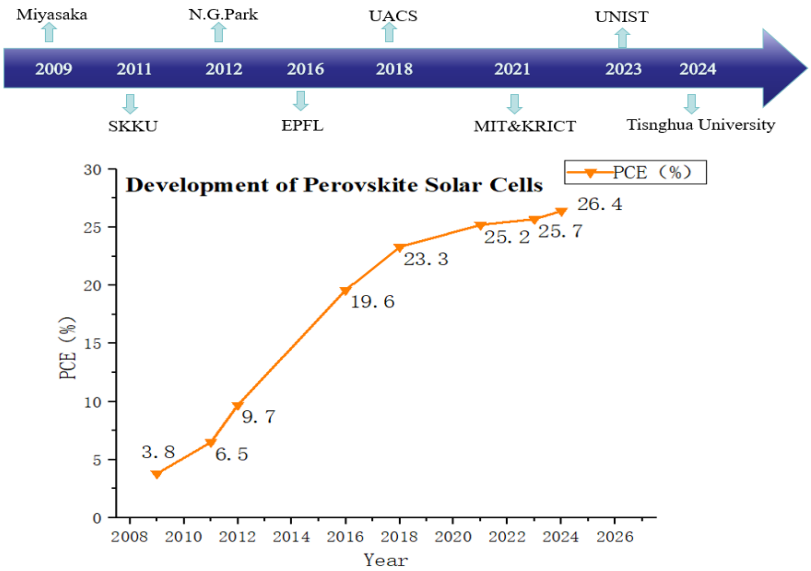

Fig 1. The Development Trends of Perovskite Solar Cells.

Reference [9] definitely increased the photoelectric conversion efficiency to 6.54% by fabricating efficient perovskite quantum dot-sensitized solar cells. Reference [10] ameliorated the photoelectric conversion efficiency to 25.2% by optimizing the electron transport layer. Reference [11] effectively reduced the charge injection barrier by combining graphene with perovskite, thereby significantly improving the electrical performance of the solar cells. Reference [12] designed and implemented flexible devices, where the flexible cells with graphene electrodes retained over 90% of their initial efficiency even after 1,000 bending cycles, achieving a photoelectric conversion efficiency of 16.8%.

Reference [13] applied graphene to transparent electrodes, electron transport layers, perovskite active layers, and passivation layers, thereby improving the photoelectric conversion efficiency, stability, and mechanical flexibility. Reference [14] introduced single-atom materials, achieving a stabilized photoelectric conversion efficiency of 20.6%.The above studies discuss strategies to improve the stability of perovskite solar cells through advancements in material design. Building on these works, this paper utilizes a perovskite solar cell simulation platform to design and implement a high-performance, temperature-adaptive, and stable perovskite solar cell based on graphene-based metamaterials, operating efficiently under solar light in the 300 nm–900 nm range.

2. The Working Principle of Solar Cells

2.1. The Impact of Graphene on the Mechanisms of Perovskite Solar Cells

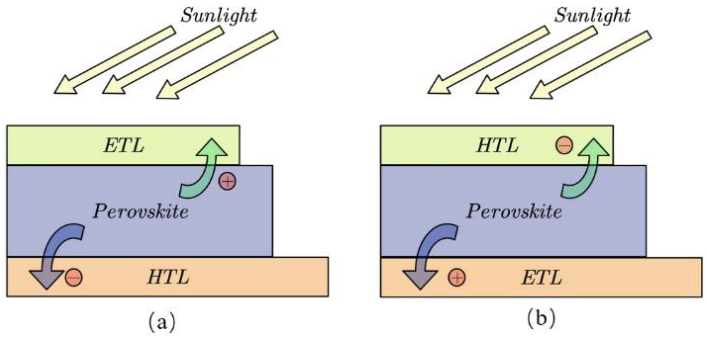

Fig 2. Perovskite working mechanism schematic diagram: (a) normal configuration, (b) inverted configuration.

After absorbing sunlight, perovskite solar cells generate electron-hole pairs. In the different structures, charge carriers move in different directions and form a pathway through the external circuit, as shown in Fig 2.

Graphene materials possess excellent optical, thermal, and mechanical properties, as well as flexible physical characteristics. The introduction of graphene offers new possibilities for designing more efficient perovskite solar cells.

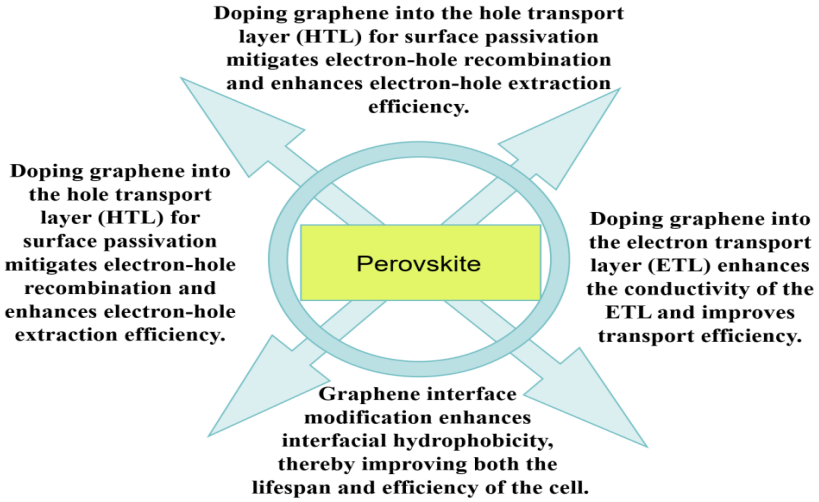

Fig 3. Applications of Graphene in the Interfaces of Perovskite Solar Cells.

In terms of electrodes, the application of graphene demonstrates excellent stability. For example, perovskite devices using graphene as an electrode material achieve a photoelectric conversion efficiency of 10.56% to 10.73% under illumination and maintain over 70% of their original efficiency after 1,000 bending cycles with a bending radius of 8 mm. When graphene is doped into the electron transport layer, it can passivate the surface of the perovskite material, slowing down the recombination process of electron-hole pairs. The role of graphene in the hole transport layer is

primarily reflected in its significant enhancement of the conductivity of the hole transport layer, thereby improving the overall current output of the cell. The high carrier mobility of graphene allows for more efficient hole transport, which helps to reduce carrier recombination losses and promote the photoelectric conversion efficiency of the cell. The carbon-based perovskite solar cells (C-PSCs) based on Ti$_1$–rGO have achieved a power conversion efficiency of up to 20.6% under steady-state conditions [14]. Furthermore, the use of graphene-based metamaterials in the design of perovskite solar cells can remarkably rise the conversion efficiency and stability of perovskite solar cells. Fig 3 also illustrates other applications of graphene in perovskite solar cells.

2.2. The Impact of Metamaterials on the Mechanisms of Perovskite Solar Cells

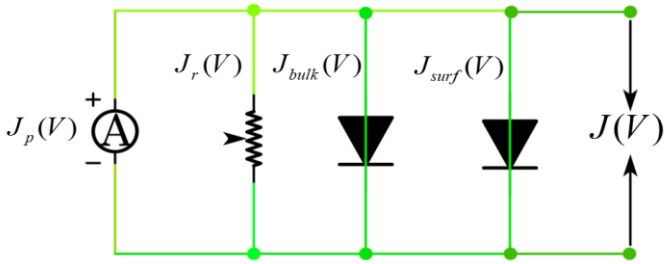

Fig 4. Schematic diagram of the internal circuit of a perovskite solar cell: $J_p(V)$ represents the photocurrent, $J_r(V)$ represents the current absorbed by the drift resistance, $J_{bulk}(V)$ represents the bulk recombination current, and $J_{surf}(V)$ represents the surface recombination current.

The internal circuit of the perovskite solar cell is shown in Fig 4, and the total current generated by the perovskite cell is expressed in Equation (1).

$$J(V) = J_p(V) - J_r(V) - J_{bulk}(V) - J_{surf}(V) - e \tag{1}$$

The calculation methods for $J_{bulk}(V)$ and $J_{surf}(V)$ in Equation (1) are shown in Equation (2), which are proportional to γ_{bulk} (bulk recombination coefficient) and γ_{surf} (surface recombination coefficient).

$$\begin{aligned} J_{bulk}(V) &= qL\gamma_{bulk} n_i \exp[\frac{q(V + JR_s)}{2k_B T}] \\ J_{surf}(V) &= qL\gamma_{surf} \frac{n_i^2}{p_0^h} \exp[\frac{q(V + JR_s)}{2k_B T}] \end{aligned} \tag{2}$$

The specific calculation methods for γ_{bulk} and γ_{surf} are shown in Equation (3).

$$\begin{aligned} \gamma_{bulk} &= \frac{np - n_i^2}{\tau_{bulkn}(p + p_t) + \tau_{bulkp}(n + n_t)} \\ \gamma_{surf} &= \frac{n^+ p^- - n_i^2}{\tau_{surfn}(p^- + p_t) + \tau_{surfp}(n^+ + n_t)} \end{aligned} \tag{3}$$

By introducing C_{60} into the perovskite solar cell to form graphene-based metamaterials, the bulk recombination and surface recombination lifetimes of the perovskite cell are improved, reducing γ_{bulk} and γ_{surf}. Based on the proportional relationship between current and coefficients (Equation (2)) and combining the current equation, this increases $J(V)$. In addition, metamaterials can lift the activation energy of HTL and ETL, thereby reducing the probability of ion migration according to Equation (4), resulting in stabilized device efficiency.

$$r_m \propto -E_A \tag{4}$$

3. Experiments and Conclusions

3.1. Conventional perovskite solar cell vs. graphene-based solar cell

Table 1. Table of parameters for non-graphene-based cells.

Non – graphene	*Parameter*	*ETL*	*Perovskite*	*HTL*
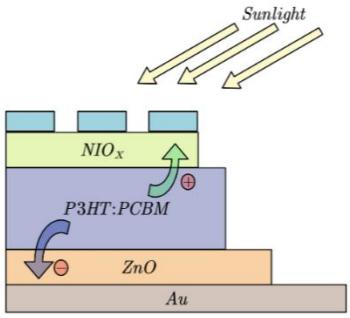	D	$20nm$	$100nm$	$40nm$
	μ_n	$3.8462cm^2/(Vs)$	$65cm^2/(Vs)$	$3.8462\times10^{-3}cm^2/(Vs)$
	μ_p	$3.8462\times10^{-2}cm^2/(Vs)$	$65cm^2/(Vs)$	$3.8462\times10^{-1}cm^2/(Vs)$
	χ	$4eV$	$3.7eV$	$3.4eV$
	E_g	$1.7eV$	$1.7eV$	$1.7eV$
	τ_n	$1000s$	$3\times10^{-11}s$	$1000s$
	τ_p	$1000s$	$3\times10^{-9}s$	$1000s$

Table 2. Table of parameters for graphene-based cells.

Graphene	*Parameter*	*ETL*	*Perovskite*	*HTL*
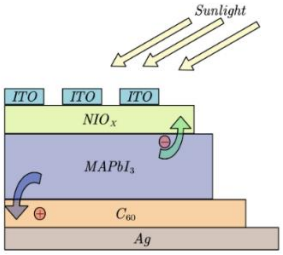	D	$20nm$	$100nm$	$40nm$
	μ_n	$3.8462cm^2/(Vs)$	$65cm^2/(Vs)$	$3.8462\times10^{-3}cm^2/(Vs)$
	μ_p	$3.8462\times10^{-2}cm^2/(Vs)$	$65cm^2/(Vs)$	$3.8462\times10^{-1}cm^2/(Vs)$
	χ	$4eV$	$3.7eV$	$3.4eV$
	E_g	$1.7eV$	$1.7eV$	$1.7eV$
	τ_n	$1000s$	$3\times10^{-11}s$	$1000s$
	τ_p	$1000s$	$3\times10^{-9}s$	$1000s$

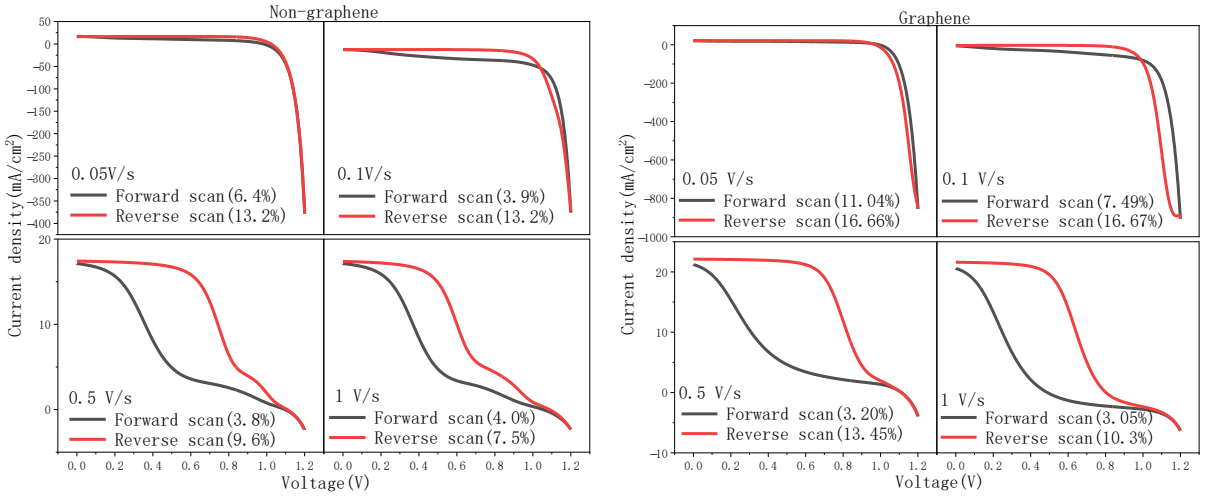

(a) (b).

Fig 5. (a) Forward and reverse scan curves of a conventional perovskite solar cell, (b) Forward and reverse scan curves of a graphene-based solar cell.

By setting up a comparative experiment between conventional cells and graphene-based cells, the changes in the efficiency of perovskite solar cells can be observed intuitively. Table 1 and Table 2 list the parameters of conventional cells and graphene-based cells, respectively. D Represents thickness, μ_n and μ_p are the electron mobility and hole mobility, respectively, χ is the electron affinity, and E_g is the bandgap energy. The material of the device is used as a control factor, and

different voltage scanning speeds are applied to obtain the relationship between current density and voltage. The scanning results are shown in Fig 5.

3.2. Result Analysis

Under different scanning speeds, both conventional perovskite solar cells and graphene-based cells exhibit similar trends. As the scanning voltage increases, the difference between the forward and reverse scans gradually widens, showing a significant hysteresis effect, which is a key issue that needs to be addressed in research. However, under the same scanning speed conditions, the efficiency of graphene-based cells is significantly higher than that of conventional perovskite solar cells. For example, at a scanning speed of 0.05 V/s, the forward scan efficiency of the graphene-based cell is 11%, and the reverse scan efficiency is 16%. In contrast, the forward scan efficiency of the conventional perovskite cell is only 6%, and the reverse scan efficiency is 13%. These data indicate that, although both types of cells exhibit hysteresis effects, the introduction of graphene elevates the overall workpiece ratio of the cells to some extent and optimizes the device performance. This characteristic provides a significant reference for the further design and optimization of perovskite solar cells.

3.3. Parameter settings for metamaterial-based cells.

Table 3. Parameter settings for metamaterial-based cells.

Metamateria	*Parameter*	*ETL*	*Perovskite*	*HTL*
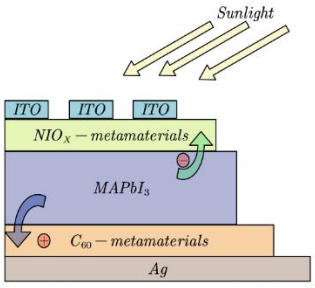	D	$20nm$	$100nm$	$40nm$
	μ_n	$3.8462cm^2/(Vs)$	$20cm^2/(Vs)$	$2\times10^{-1}cm^2/(Vs)$
	μ_p	$3.8462\times10^{-2}cm^2/(Vs)$	$20cm^2/(Vs)$	$20cm^2/(Vs)$
	χ	$4eV$	$3.8eV$	$2.8eV$
	E_g	$1.7eV$	$1.6eV$	$2.3eV$
	τ_n	$1\times10^{-6}s$	$1\times10^{-6}s$	$1\times10^{-6}s$
	τ_p	$1\times10^{-6}s$	$1\times10^{-6}s$	$1\times10^{-6}s$

3.4. Band structure of metamaterial-based cells.

The holes migrate from the valence band of the perovskite active layer to NiO_x, and then to the ITO electrode. Meanwhile, the electrons migrate from the conduction band of the perovskite layer to the C_{60} layer and are finally transported to the Ag electrode, as shown in Fig 6.

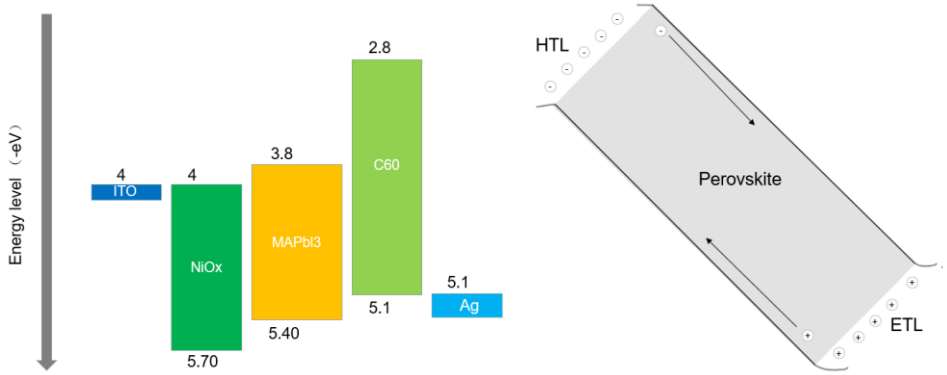

(a) (b)

Fig 6. Device structure diagram: (a) Band structure diagram of the device, (b) Schematic diagram of electron and hole movement in the active layer.

The conduction bands of ITO and NiO_x layer are perfectly aligned, reducing the energy barrier for hole injection. The conduction band of $MAPbI_3$ layer is 3.8 eV, and its valence band is

5.4 eV, which aligns well with the valence band of NiO_x, facilitating whole migration from the active layer to the HTL layer. The energy level of the electron transport layer (C_{60}, conduction band of 2.8 eV) forms a reasonable barrier with the conduction band of $MAPbI_3$ layer, effectively blocking the backflow of holes. This band step structure also promotes electron transport efficiency.

3.5. The J-V characteristics of metamaterial-based cells.

Under scanning speeds of 0.05, 0.1, 0.5, and 1 V/s, the device was scanned from 0 V to 1.5 V, yielding current density-voltage (J-V) curves. As observed in Fig 7, the difference between the forward and reverse scans is minimal, almost overlapping, indicating that the designed metamaterial exhibits excellent charge extraction and transport properties, with the hysteresis effect remarkably suppressed. Moreover, Fig 7 shows that under different scanning speed conditions, the device efficiency remains stable between 19.8% and 20.4%, demonstrating outstanding stability. The workpiece ratio of the metamaterial-based perovskite solar cell consistently remains at approximately 20%, which is significantly higher than that of conventional perovskite solar cells and also superior to the performance of graphene-based cells. This indicates that the design of the metamaterial offers significant advantages in improving perovskite cell efficiency and suppressing the hysteresis effect.

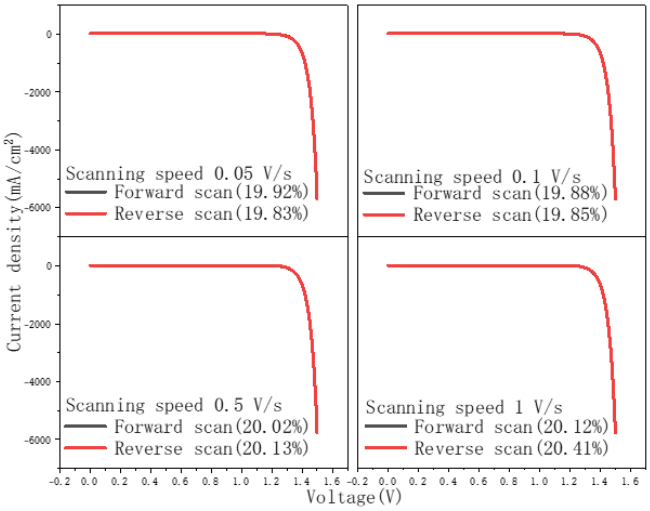

Fig 7. The J-V characteristic curves of metamaterial-based devices under different scanning speeds.

3.6. Steady-State Analysis of Metamaterial-Based Cells.

The steady-state voltage is set to 1.2V. According to Fig 8, we can observe the distribution of ion concentration and device spatial coordinates.

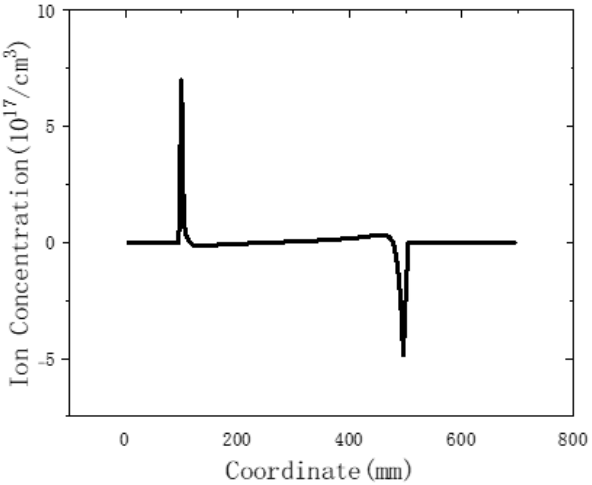

Fig 8. The net ion concentration distribution diagram of the device.

At spatial coordinates around 100 nm and 500 nm, positive and negative peaks are observed, indicating significant charge accumulation in the interfacial regions. In the central region, the ion concentration approaches zero, suggesting that the positive and negative charge concentrations in the perovskite region cancel each other out, resulting in a near-equilibrium state. This demonstrates that ion migration has reached a steady state, forming a conductive pathway.

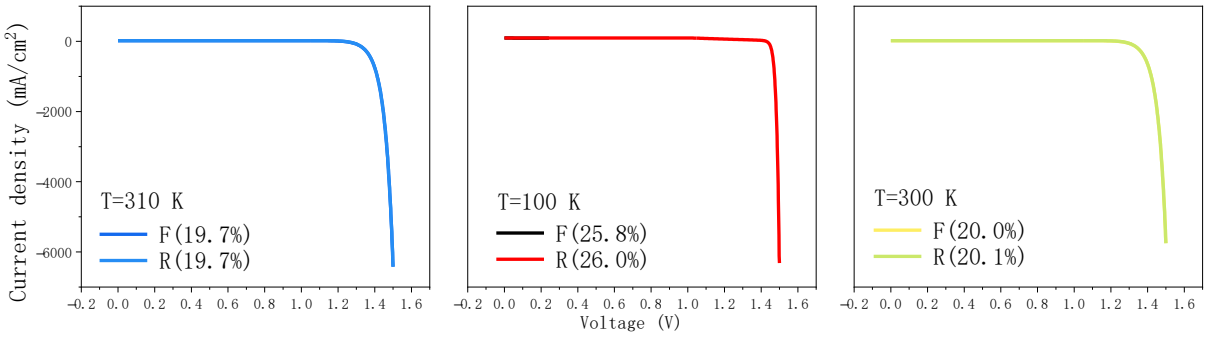

Fig 9. The efficiency performance of the device under different temperatures.

By comparing the performance of the device at different temperatures, it is observed that the conversion efficiency shows a certain downward trend as the temperature increases. Simultaneously, noise increases with rising temperatures, interfering with the device's stability. However, experimental results indicate that the device still exhibits excellent performance stability under extreme temperature conditions. As shown in Fig 9, at a temperature of 310 K, the conversion efficiency is around 19.7%, maintaining 98% of its original efficiency. At 100 K, the cell's conversion efficiency increases to 25.9%. This demonstrates that the device performs well under both low-temperature and high-temperature extreme environments.

4. Discussion

In comparison with conventional graphene materials, graphene metamaterials have been shown to exhibit increased energy band alignment compatibility with chalcogenides, reduced energy barriers for carrier injection, and augmented transport workpiece ratio. This paper proposes an optimal energy band structure that has been determined through a comprehensive series of simulation experiments. This structure has been demonstrated to engender substantial enhancements in the stability, photovoltaic conversion efficiency, and temperature adaptability of sulfur solar cells, while concurrently suppressing ion migration. The design of an efficient and stable perovskite solar cell is also presented. The innovation points of this paper are as follows:

Metamaterial and structure design: graphene-based metamaterials are aligned with the energy bands of chalcogenide materials with a view to reducing ion migration, optimising carrier transport, reducing compound losses and improving stability and workpiece ratio.

High conversion rate: As shown in Fig 9, the cell workpiece ratio is stable at extreme temperatures (100 K-310 K), with 19.7% efficiency at 310 K (maintaining 98%) and 25.9% efficiency at 100 K, showing strong environmental adaptability and stability.

Stability: The forward and reverse scanning curves of graphene-based metamaterial cells almost overlap at different scanning speeds (0.05-1 V/s), remarkably suppressing the J-V hysteresis.

5. Conclusion

This study designs a graphene-based metamaterial perovskite solar cell and compares it with traditional perovskite cells and graphene-based cells, verifying the positive impact of graphene introduction on improving cell performance. Experimental results show that the photoelectric conversion efficiency of graphene-based cells increases from 13.2% to 16.7%. However, both types

of cells exhibit significant J-V hysteresis, which affects their normal operation. To address this issue, a graphene-based metamaterial perovskite cell was designed.

After introducing the metamaterial, the device demonstrated outstanding performance. J-V characteristics reveal that the forward and reverse scans of the metamaterial device almost completely overlap, with significantly reduced hysteresis compared to traditional perovskite cells and graphene-based cells. In the steady-state analysis, the introduction of the metamaterial significantly reduced ion migration rates and extended the carrier recombination lifetime of the perovskite material, greatly enhancing device stability. Furthermore, under extreme environmental testing (low temperature of 100 K and high temperature of 310 K), the metamaterial cell maintained excellent photoelectric conversion performance. Notably, at high temperatures (310 K), the device retained 98% of its conversion efficiency, fully demonstrating its strong environmental adaptability. Its workpiece ratio remains stable between 19.7 % (310 K) and 25.05 % (100K). The application of graphene-based metamaterials provides an important reference for improving the stability and photoelectric conversion efficiency of perovskite solar cells.

References

[1] Akihiro K ,Kenjiro T ,Yasuo S , et al.Organometal halide perovskites as visible-light sensitizers for photovoltaic cells.[J].Journal of the American Chemical Society,2009,131(17):6050-1.

[2] Jeong-Hyeok I ,Chang-Ryul L ,Jin-Wook L , et al.6.5% efficient perovskite quantum-dot-sensitized solar cell.[J].Nanoscale,2011,3(10):4088-93.

[3] Hui-Seon K ,Chang-Ryul L ,Jeong-Hyeok I , et al.Lead iodide perovskite sensitized all-solid-state submicron thin film mesoscopic solar cell with efficiency exceeding 9%.[J].Scientific reports,2012,2(1):591.

[4] Li X ,Bi D ,Yi C , et al.A vacuum flash–assisted solution process for high-efficiency large-area perovskite solar cells[J].Science, 2016, 353(6294):58-62.

[5] Liang C ,Zhao D ,Li Y , et al.Ruddlesden–Popper Perovskite for Stable Solar Cells[J].Energy & Environmental Materials, 2018, 1(4):221-231.

[6] Hwan G K ,Suk D K .Development of perovskite solar cells with 25% conversion efficiency[J].Joule,2021,5(5):1033-1035.

[7] Jaewang P ,Jongbeom K ,HyunSung Y , et al.Controlled growth of perovskite layers with volatile alkylammonium chlorides.[J].Nature,2023,616(7958):724-730.

[8] Zhou J, Tan L, Liu Y, ET al.Highly efficient and stable perovskite solar cells via a multifunctional hole transporting material [J].Joule, 2024, 8(6):1691-1706.

[9] Jeong-Hyeok Im, Lee, Chang-Ryul Lee, Jin-Wook Lee, Sang-Won Park, Nam-Gyu Park.6.5% efficient perovskite quantum-dot-sensitized solar cell[J]. Nanoscale, 2011, 3(9):4088-4093.

[10] Jason J. Yoo, Gabkyung Seo, Matthew R. Chua, et al. Efficient perovskite solar cells via improved carrier management [J]. Nature, 2021, 590(7847): 587-592.

[11] Kai Leng, Lin Wang, Yan Shao, et al. Electron tunneling at the molecularly thin 2D perovskite and graphene van der Waals interface[J]. *Nature Communications*, 2020, 11: Article 5483.

[12] Jungjin Yoon, Hyangki Sung, Gunhee Lee, Woohyung Cho, Namyoung Ahn, Hyun Suk Jung, Mansoo Choi. Super flexible, high-efficiency perovskite solar cells employing graphene electrodes: Toward future foldable power sources [J]. *Energy & Environmental Science*. 2016.

[13] Kaiwen Gong, Jichao Hu, Nan Cui, et al. The roles of graphene and its derivatives in perovskite solar cells: A review. *Materials & Design* [J], 2021, 211: 110170.

[14] Chunyang Zhang, Suxia Liang, Wei Liu, et al. Ti1–graphene single-atom material for improved energy level alignment in perovskite solar cells [J]. *Nature Energy*, 2021, 6(12): 1154-1163.